

# Magnesium-Enhanced Reactivity of Boron Particles: Role of Mg/B<sub>2</sub>O<sub>3</sub> Exothermic Surface Reactions

Pankaj Ghildiyal, Feiyu Xu, Alex Rojas, Yujie Wang, Mahbub Chowdhury, Prithwish Biswas, Steven Herrera, Reza Abbaschian,\* and Michael R. Zachariah\*



Cite This: *Energy Fuels* 2023, 37, 3272–3279



Read Online

ACCESS |



Metrics & More

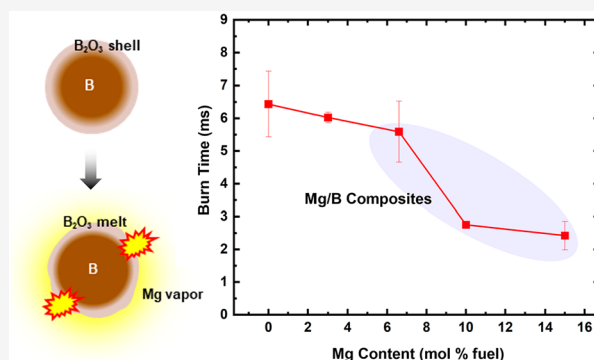


Article Recommendations



Supporting Information

**ABSTRACT:** Boron offers great promise as a candidate fuel in high-energy composites as a result of its high gravimetric and volumetric energy content; however, its oxidation rate is limited by sluggish diffusion of reactive species across its low-melting oxide shell. On the other hand, Mg nanoparticles (NPs) have been shown recently to undergo fast oxidation following rapid vaporization ( $\sim 100 \mu\text{s}$  at high heating rates of  $\sim 10^5 \text{ }^\circ\text{C/s}$ ). This release of vapor-phase Mg can potentially be exploited to react exothermically ( $\Delta H_r = -420 \text{ kJ/mol}$ ) with the B<sub>2</sub>O<sub>3</sub> layer of boron, inducing surface disruptions and promoting its combustion. In this paper, we explore this effect by evaluating Mg NPs as additive fuel to B/CuO nanoenergetic composites. We observe that incorporating Mg as an additive fuel in B/CuO composites results in a  $\sim 6$ -fold enhancement in reactivity with a  $\sim 60\%$  reduction in burn time. Through thermal and reaction product analysis along with high-speed time-of-flight mass spectrometry (T-jump/TOFMS) and ignition characterization, we investigate the reaction mechanism of Mg/B<sub>2</sub>O<sub>3</sub> particles as a simulat system for the interaction of Mg with the B<sub>2</sub>O<sub>3</sub> shell of boron. These characterizations reveal that exothermic heterogeneous reactions occur between vapor-phase Mg and the molten B<sub>2</sub>O<sub>3</sub> shell of boron at  $\sim 500$ – $650 \text{ }^\circ\text{C}$ . The role of these exothermic surface reactions in inducing surface modifications and reactivity enhancement of boron particles is discussed.



## 1. INTRODUCTION

Nanoscale metals and metalloids, such as Al, Ti, Mg, B, and Si, have been explored as high-energy fuels in nanoenergetic composites for propellant and pyrotechnic applications.<sup>1–5</sup> Among these fuels, boron has always been regarded as the premier candidate fuel as a result of its higher gravimetric and volumetric reaction enthalpies,<sup>6</sup> as shown in Figure 1. Despite its thermodynamic advantages over other fuels, boron suffers from sluggish oxidation and energy release kinetics as a result of its low-melting oxide shell (B<sub>2</sub>O<sub>3</sub>, with a melting point of  $\sim 450 \text{ }^\circ\text{C}$ ).<sup>6–9</sup> Post-melting, the non-volatile liquid oxide layer (boiling point of  $\sim 1860 \text{ }^\circ\text{C}$ ) acts as a diffusion barrier to the oxidizing species and restricts their access to the B core, thereby significantly inhibiting B oxidation and energy release.<sup>6,9</sup> Several surface modification strategies, such as oxide removal by solvent washing,<sup>10</sup> surface functionalization with fluorine-based organic,<sup>11</sup> polymeric, and graphitic moieties,<sup>12</sup> and incorporation of fluoride salts,<sup>5,13</sup> have been explored to alter or remove the oxide surface of boron to promote its ignition and combustion characteristics.

Alternatively, exploring binary fuel systems by incorporating energy-dense metal additives, such as Al, Mg, and Ti, in boron powders has been demonstrated as a promising strategy to accelerate B oxidation while maintaining a high energetic

content.<sup>14–17</sup> Employing similar dual fuel systems has been used to control and modulate the transport processes and ignition in thermite mixtures.<sup>18,19</sup> Among the metal additives explored thus far, Mg is particularly attractive as a result of its high volatility and reactivity. In our previous work on Mg nanoparticle (NP)-based thermites, we have shown that reducing the particle size of Mg NPs results in their rapid vaporization and a fast vapor-phase Mg release (release time scale of  $\sim 100 \mu\text{s}$  at a heating rate of  $10^5 \text{ }^\circ\text{C/s}$ ).<sup>20</sup> Additionally, as a result of the highly negative formation energies of MgO compared to B<sub>2</sub>O<sub>3</sub> (Mg lies lower than B in the Ellingham diagram), the reaction between Mg and B<sub>2</sub>O<sub>3</sub> is thermodynamically feasible with a reaction enthalpy ( $\Delta H_r$ ) of  $\sim -420 \text{ kJ/mol}$  or  $-2.9 \text{ kJ/g}$ . Therefore, Mg NPs, as an additive fuel, can offer a thermodynamically and kinetically viable source of highly reactive gas-phase Mg that can potentially act as an

Received: July 16, 2022

Revised: January 10, 2023

Published: January 30, 2023



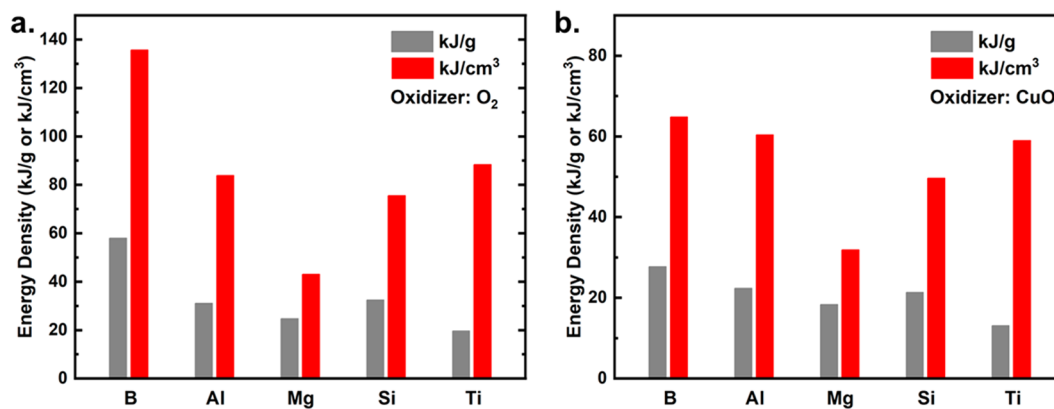
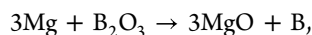


**Figure 1.** Comparison of volumetric and gravimetric energy densities of boron to other fuels considering a stoichiometric reaction with the oxidizers: (a) oxygen and (b) CuO. The energy density is calculated as the reaction enthalpy per unit mass or volume of the fuel.

etchant for the oxide shell of boron according to the following reaction:



$$\Delta H_r = -420 \text{ kJ/mol}_{\text{reaction}}$$

Previous studies have reported that coating boron with materials (e.g., fluorographene and fluoroalkylsilanes) that can release gas-phase fluorine species to etch the  $\text{B}_2\text{O}_3$  shell promotes its ignition and combustion.<sup>11,12</sup> Similarly, nanoscale Mg can provide these advantages by generating reactive gas-phase species (Mg vapor) to corrode the oxide shell while maintaining a high energy density of the composites. Although prior studies have explored the role of Mg as an additive in B-based powders,<sup>16,17,21</sup> these reports have been limited to micrometer-scale Mg powders that, as a result of their low surface area, are expected to have slow vaporization and release kinetics of gas-phase Mg species. Furthermore, the mechanisms and synergistic effects of the surface reaction of Mg vapor directly with the oxide shell of boron have not been investigated.

In this study, we first fabricate and evaluate the energy release characteristics of B/CuO composites with Mg NPs ( $\sim 370$  nm) incorporated as an additive fuel with loadings ranging from  $\sim 3$  to 15 mol % of the total fuel. We demonstrate that incorporating Mg in B/CuO thermite results in up to 6-fold higher pressurization rates and  $\sim 60\%$  reduction in burn times of the composites. Through a combination of differential scanning calorimetry (DSC), reaction product characterization, and high-speed time-of-flight mass spectrometry (T-jump/TOFMS), we probe the mechanism of the reaction between Mg and  $\text{B}_2\text{O}_3$  particles. These characterizations reveal that the mechanism of the Mg– $\text{B}_2\text{O}_3$  interaction involves an exothermic redox reaction between vapor-phase Mg and molten  $\text{B}_2\text{O}_3$ . The role and potential physical effects of these reactions in inducing surface disruptions in boron particles and promoting their combustion is further discussed.

## 2. EXPERIMENTAL SECTION

**2.1. Materials.** Boron [ $\sim 410$  nm as measured from the scanning electron microscopy (SEM) in Figure S1a of the Supporting Information, with 80% active B content] and copper oxide nanoparticles (CuO,  $\sim 40$  nm) were obtained from U.S. Research Nanomaterials. Mg NPs were prepared by an electromagnetic levitation technique, described in our previous work.<sup>20</sup> Briefly, a  $\sim 0.35$  g spheroidal Mg piece was levitated and heated to  $\sim 993$  K in a

purified Ar/He gas flow. Mg NPs were recovered downstream from the particle-laden gas on a Millipore Sigma polycarbonate membrane filter ( $0.3 \mu\text{m}$  pore diameter). The average particle size of the synthesized Mg NPs was  $\sim 370$  nm, as shown in Figure S1b of the Supporting Information, while the active Mg content was estimated to be  $\sim 88\%$ . The active content of the fuels (B and Mg) was estimated from the mass gain upon oxidation in air or  $\text{O}_2$  (see section S2 of the Supporting Information). Boron oxide ( $\text{B}_2\text{O}_3$ ) was purchased from Alfa Aesar and was ball-milled to reduce the particle size to  $\sim 2 \mu\text{m}$ , as described in section S3 of the Supporting Information.

**2.2. Preparation of Nanothermite Composites.** The B–Mg/CuO nanothermite composites were prepared by adding the fuel and oxidizer components in hexane (10 mg/mL solid loading) followed by  $\sim 1$  h of ultrasonication to achieve homogeneous particle mixing. The samples were then dried for 24 h under ambient conditions to obtain the thermite powders. For these composites, incremental amounts of Mg particles were added while a constant B/CuO mass ratio was maintained to achieve a fuel/oxidizer equivalence ratio of 1 (B/CuO,  $\phi = 1$ ). The composition of the formulations fabricated have been tabulated in Table S1 in section S4 of the Supporting Information. Constant-volume combustion cell ( $\sim 20 \text{ cm}^3$ ) characterization was performed on 25.0 mg of the samples using the setup described in prior works.<sup>20,22</sup>

**2.3. Material Characterization.** Microscopic characterization of the samples was performed on a FEI NNS450 microscope operating at 18 kV. Constant-volume combustion cell ( $\sim 20 \text{ cm}^3$ ) measurements were performed on 25.0 mg of the fabricated thermite composites using a setup described in our previous studies.<sup>20,22</sup> For thermogravimetric analysis and differential scanning calorimetry (TGA/DSC), a Netsch STA449 F3 Jupiter thermal analyzer was used. Ultrahigh-purity argon (purity of  $\sim 99.9999\%$ ) was used as the TGA atmosphere to prevent Mg particle oxidation. X-ray diffraction (XRD) on the samples was performed with a PANalytical Empyrean Series 2 diffractometer (Cu  $K\alpha$  radiation). Attenuated total reflection–Fourier transform infrared (ATR–FTIR) characterization on the samples was performed on a Nicolet iS50R spectrometer with a deuterated triglycine sulfate (DTGS) detector with a  $4 \text{ cm}^{-1}$  resolution. Crushed and dried KBr was used as a reference, and the spectra obtained were processed using Happ–Genzel apodization, Mertz phase correction, and atmospheric suppression.

**2.4. T-Jump/TOFMS and Ignition Characterization.** T-Jump/TOFMS and ignition temperature characterizations were performed to probe and investigate the reaction mechanisms in the fabricated composites at high heating rates ( $\sim 10^5 \text{ K s}^{-1}$ ), as detailed elsewhere.<sup>22,23</sup> Briefly, a small quantity ( $\sim 5$  mg) of the prepared composites was dispersed in hexane and sonicated for  $\sim 10$  min. The suspension was then drop-cast on a platinum wire ( $\sim 1$  cm,  $76 \mu\text{m}$  diameter) soldered to copper leads of the electrical feedthroughs. The samples were then heated with a  $\sim 3$  ms pulse under a high vacuum ( $10^{-9}$  atm) to a maximum temperature of  $\sim 1400$  K. Following

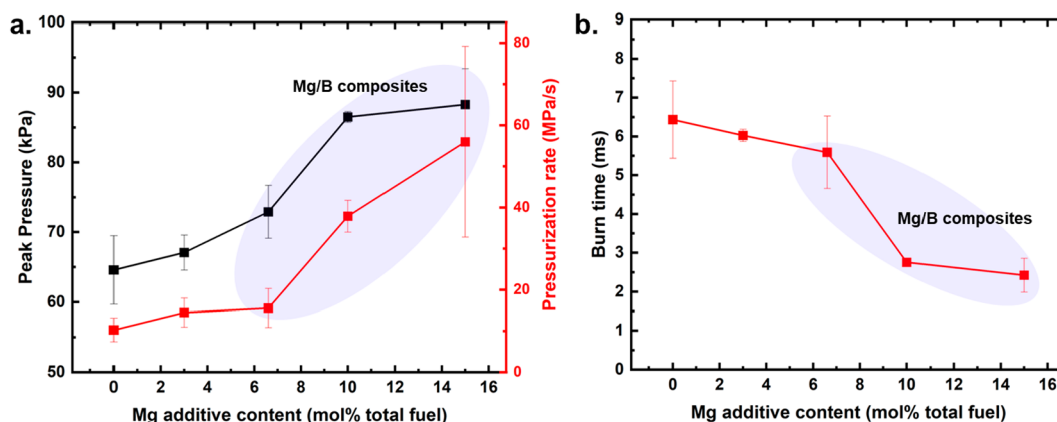


**Figure 2.** Effect of Mg addition on (a) peak pressure and pressurization rate and (b) burn characteristics of B/CuO nanoenergetic composites. Mg/B/CuO composites show significant enhancement in burn times and pressurization over B/CuO thermites.

**Table 1. Thermochemistry and Ignition Temperature Measurements Obtained for Different Possible Reactive Systems Involved in B/Mg/CuO Combustion<sup>a</sup>**

reactive system	reaction	$\Delta H_{rm}$ (kJ mol <sup>-1</sup> )	$\Delta H_{rg}$ (kJ g <sup>-1</sup> )	ignition temperature ( $\pm 40$ °C)
B/CuO <sup>27</sup>	2B + 3CuO $\rightarrow$ B <sub>2</sub> O <sub>3</sub> + 3Cu (i)	-780	-3.0	760
Mg/CuO <sup>27</sup>	Mg + CuO $\rightarrow$ MgO + Cu (ii)	-440	-4.3	800
B/Mg/CuO	i, ii, iii, and iv			730
Mg/B <sub>2</sub> O <sub>3</sub> <sup>27</sup>	3Mg + B <sub>2</sub> O <sub>3</sub> $\rightarrow$ 3MgO + Cu (iii)	-550	-3.9	600
MgO/B <sub>2</sub> O <sub>3</sub> <sup>28</sup>	3MgO + B <sub>2</sub> O <sub>3</sub> $\rightarrow$ Mg <sub>3</sub> B <sub>2</sub> O <sub>6</sub> (iv)	-110	-0.6	

<sup>a</sup> $\Delta H_{rm}$  and  $\Delta H_{rg}$  represent the molar and gravimetric reaction enthalpies. Enthalpy values are calculated from the references mentioned.

thermal activation by the pulse, the gas-phase species evolved during the reaction were ionized with a 70 eV electron gun and probed with a multichannel plate detector for 10 ms with a temporal resolution of 100  $\mu$ s. The ignition characterization of the samples was carried out with a high-speed camera (Vision Research Phantom, version 12.0) in an argon environment at 1 atm pressure. The ignition point was identified by correlating the optical emission obtained from the camera with the time and temperature obtained from wire heating.

### 3. RESULTS AND DISCUSSION

**3.1. Effect of Mg Addition on the Energetic Characteristics of B/CuO Composites.** First, we explore the effect of Mg NPs as an additive fuel on the reactivity and energy release of boron NP-based composites. To evaluate this effect, we first fabricated B/Mg/CuO nanoenergetic composites with a varying additive content of Mg NPs and

characterized their pressurization characteristics by constant-volume combustion cell measurements, as described in our previous work.<sup>20</sup> Figure 2 and Figure S4 of the Supporting Information show the measured reactivity parameters (peak pressures, pressurization rates, and burn times) of B/Mg/CuO composites at different additive Mg loadings. Clearly, increasing the Mg content results in enhanced reactivity of the composites with higher peak pressures and pressurization rates and shorter burn times. Notably, Mg/B-based composites show up to  $\sim 6$ -fold enhancement in pressurization rates and a  $\sim 30\%$  increase in peak pressures relative to B-based composites (Figure 2a). Additionally, Mg addition to B/CuO thermites shortens their burn time from  $\sim 6.5$  to  $\sim 2$  ms ( $\sim 60\%$  reduction), as shown in Figure 2b. The considerable reduction in the pressurization and burning time scales suggests that adding Mg to B-based composites augments their reaction kinetics. Importantly, Mg-based composites (without B) fabricated with the highest additive Mg amount (15 mol %) do not ignite or show pressurization with CuO. This observation is as expected because, from a compositional perspective, these composites would be highly fuel-lean because Mg is only a minor additive fuel in these composites.

On the basis of these observations, the reactivity enhancement in Mg/B samples relative to Mg- or B-based composites suggests that a synergistic effect between Mg and B fuels is likely responsible for the augmentation observed in Figure 2. As mentioned earlier, the oxidation and energy release kinetics for boron are limited and greatly affected by the transport processes occurring through its oxide shell (B<sub>2</sub>O<sub>3</sub>). Earlier studies have proposed various species (e.g., gas-phase fluorinated species and H<sub>2</sub>O vapor) that can react with and breach the molten B<sub>2</sub>O<sub>3</sub> shell, resulting in enhanced combustion of B particles.<sup>7,12,24–26</sup> As discussed earlier, the reaction between Mg and the B<sub>2</sub>O<sub>3</sub> shell of boron is

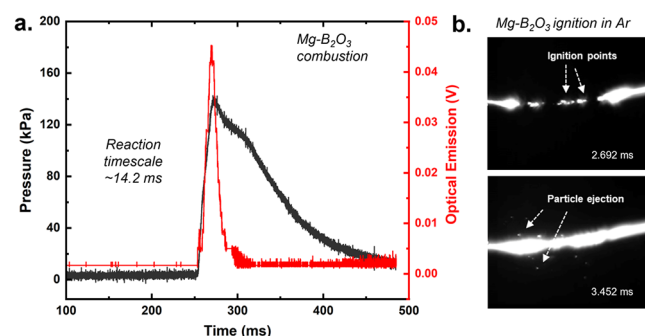


**Figure 3.** (a) Pressure and optical traces of the combustion of Mg with B<sub>2</sub>O<sub>3</sub> particles (simulant for the oxide shell of B NPs), and (b) snapshots of Mg/B<sub>2</sub>O<sub>3</sub> ignition in argon (ignition temperature = 600 °C). The timestamps in the images represent the time elapsed after triggering.

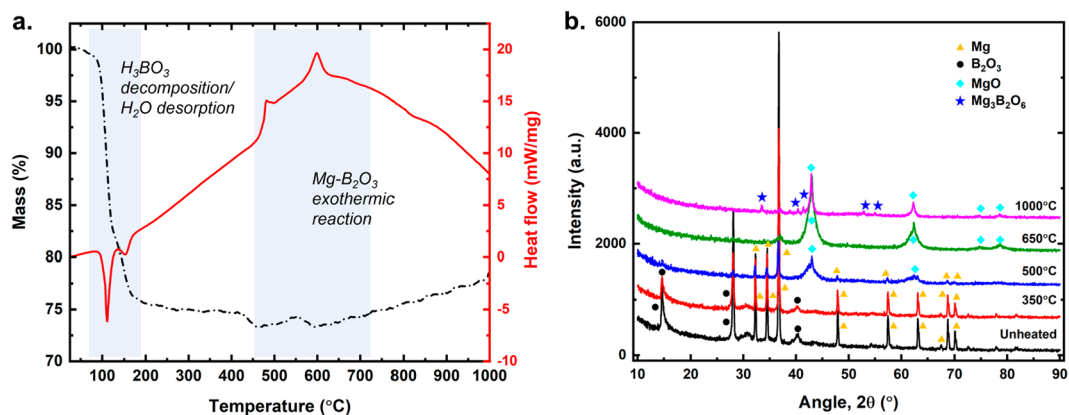


**Figure 4.** (a) TGA/DSC of Mg NPs mixed with stoichiometric  $B_2O_3$ , showing decomposition followed by an exothermic reduction of  $B_2O_3$  particulates, and (b) XRD patterns of Mg/ $B_2O_3$  samples heated at different temperatures, with the magnesiothermic reduction of  $B_2O_3$  occurring at  $\sim 500$ – $650$  °C.

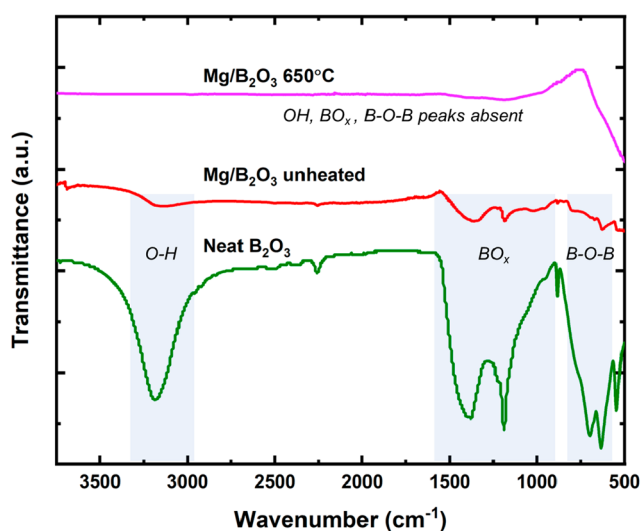


**Figure 5.** ATR-FTIR spectra of neat  $B_2O_3$ , unheated Mg/ $B_2O_3$  composites, and Mg/ $B_2O_3$  samples heated at 650 °C.

exothermic and might be involved in the combustion of Mg/B-based composites. Table 1 lists the potential reactions involved in the combustion of B-, Mg-, and mixed B-/Mg-based reactive systems. Notably, the exothermicity of the Mg/ $B_2O_3$  reaction ( $\Delta H \sim -550$  kJ mol<sup>-1</sup>) is on par with that of the Mg/CuO

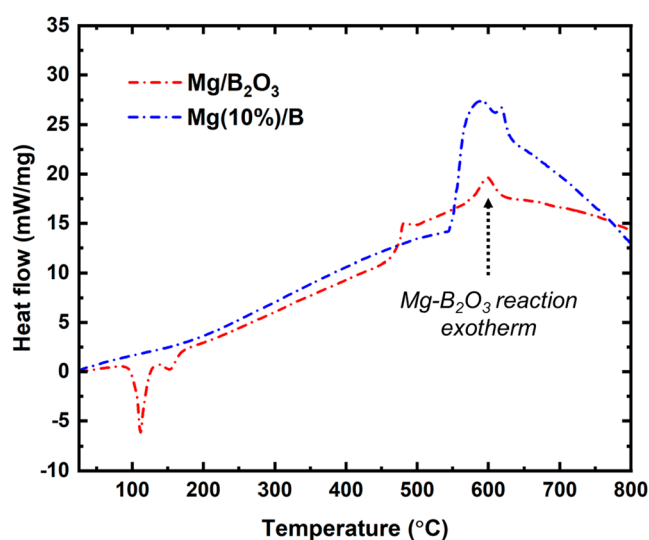


**Figure 7.** DSC of Mg/ $B_2O_3$  and Mg/B mixtures in argon, showing coinciding exothermic peaks of Mg/B and Mg/ $B_2O_3$  reaction exotherms. The Mg/B sample represents  $\sim 10$  mol % Mg with respect to the total mixture.

( $\Delta H \sim -440$  kJ mol<sup>-1</sup>) and B/CuO ( $\Delta H \sim -600$  kJ mol<sup>-1</sup>) systems on both a molar and gravimetric basis, as shown in Table 1. Therefore, from an energetic standpoint, the Mg/

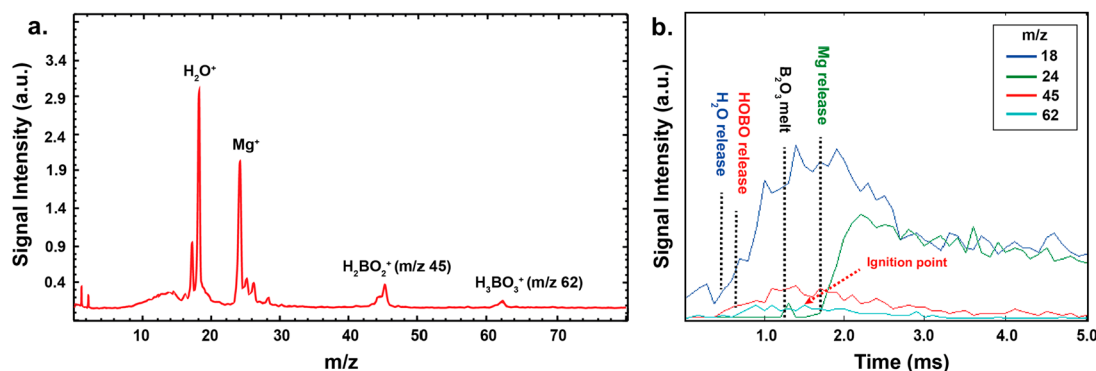


**Figure 6.** (a) T-jump/TOFMS spectrum showing  $H_2O$ , HOBO, and vapor-phase Mg species evolved from rapid heating of Mg/ $B_2O_3$  and (b) temporal evolution of different species evolved from the Mg/ $B_2O_3$  reaction as obtained from T-jump/TOFMS.

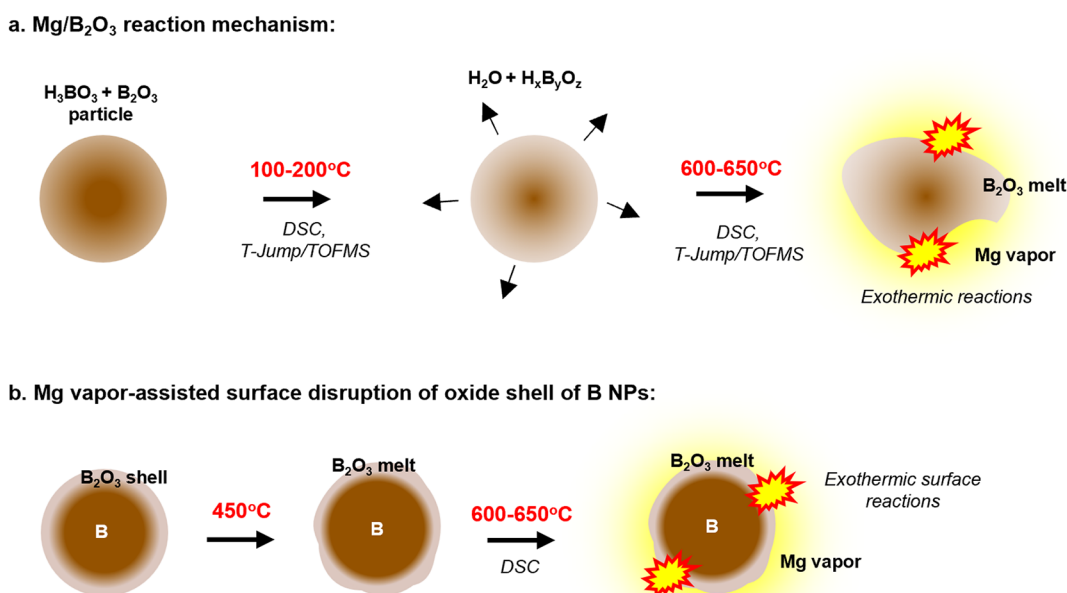


**Figure 8.** Schematic illustrating the interfacial reactions involved in Mg–B-based systems: (a) Mg vapor-induced mechanism of the Mg/B<sub>2</sub>O<sub>3</sub> reaction and (b) proposed Mg vapor-induced oxide etching and removal mechanism for B NPs likely responsible for reactivity enhancement.

B<sub>2</sub>O<sub>3</sub> reaction could contribute significantly to the overall energy release of B-based composites and needs to be taken into consideration.

To probe this reaction and its implications on reactivity enhancement of B NPs, we investigated the reaction mechanism of the Mg/B<sub>2</sub>O<sub>3</sub> reaction, which we used as a simulant for the interaction of Mg with the oxide shell of boron (B<sub>2</sub>O<sub>3</sub>). First, we fabricated Mg/B<sub>2</sub>O<sub>3</sub> composites assuming a stoichiometric redox reaction between the components ( $\phi = 1$ ) and evaluated their constant-volume pressurization and ignition characteristics. As shown in Figure 3b, the Mg/B<sub>2</sub>O<sub>3</sub> reaction initiation occurs at a relatively low temperature (ignition temperature of  $\sim 600$  °C). Interestingly, the Mg/B<sub>2</sub>O<sub>3</sub> thermite system shows significant pressurization with a peak pressure of  $\sim 130$  kPa and a pressurization rate of  $\sim 8$  MPa/s, as shown in Figure 3a. For comparison, B/CuO thermites show  $\sim 65$  kPa maximum pressure and  $\sim 10$  MPa/s pressurization rate, on par with the Mg/B<sub>2</sub>O<sub>3</sub> reactive system. Notably, the burn time of the Mg/B<sub>2</sub>O<sub>3</sub> mixture ( $\sim 14.2$  ms) is on the same order of magnitude as that of the B/CuO samples ( $\sim 6.5$  ms; Figure 2b). Note that the B<sub>2</sub>O<sub>3</sub> particles are much larger ( $\sim 2$   $\mu\text{m}$ ) than the B<sub>2</sub>O<sub>3</sub> shell on B NPs, which is expected to be on the order of tens of nanometers. Therefore, the reaction of Mg with the oxide shell is likely much faster than that for the simulant B<sub>2</sub>O<sub>3</sub> particles. Nonetheless, these results indicate that both Mg/B<sub>2</sub>O<sub>3</sub> and B/CuO reactions occur on a similar time scale, suggesting that, from a kinetic perspective, Mg can potentially interact with the oxide shell (B<sub>2</sub>O<sub>3</sub>) of boron NPs in B/Mg-based composites (Figure 2). The mechanism and further analysis of the Mg/B<sub>2</sub>O<sub>3</sub> reaction and its implications on inducing disruptions in the surface oxide of B NPs for reaction rate enhancement are discussed in the subsequent sections.

**3.2. Mg/B<sub>2</sub>O<sub>3</sub> Reaction Mechanisms: Ignition, Thermal Analysis, and Reaction Product Characterization.** Table 1 summarizes the reactions and the associated thermochemistry potentially involved in the B/Mg/CuO

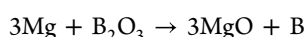
thermite system. As mentioned earlier, the reaction of Mg with CuO and B<sub>2</sub>O<sub>3</sub> are energetically comparable on both a gravimetric and molar basis (Table 1). Figure S5 of the Supporting Information shows the ignition snapshots of B/CuO, Mg/CuO, and B/Mg (15%)/CuO mixtures in an argon atmosphere. The ignition temperatures of these mixtures, summarized in Table 1, show a marginal decrease in the ignition temperature of B/Mg/CuO samples relative to B/CuO and Mg/CuO composites. More importantly, the ignition temperature of the Mg/B<sub>2</sub>O<sub>3</sub> reaction is significantly lower than that of B/CuO, Mg/CuO, and B/Mg/CuO mixtures (Figure 3 and Figure S6 of the Supporting Information). A previous study from our group has shown that the energetic reactions with Mg are initiated by the release of Mg vapor.<sup>20</sup> Therefore, the lower ignition temperature for the Mg/B<sub>2</sub>O<sub>3</sub> system ( $\sim 600$  °C) could be attributed to the molten B<sub>2</sub>O<sub>3</sub> surface (melting point of  $\sim 450$  °C) that acts as a favorable condensation site for Mg vapor to react with the oxidizer. On the other hand, the reaction of Mg vapor with CuO is limited by the release of gas-phase O<sub>2</sub> following oxidizer decomposition at higher temperatures ( $\sim 700$  °C), resulting in significantly higher ignition thresholds ( $>700$  °C).

Although the contribution from the Mg/CuO reaction cannot be completely neglected, we note that, thermodynamically, Mg has relatively similar molar and gravimetric reaction enthalpies with both CuO and B<sub>2</sub>O<sub>3</sub>, as shown in Table 1. Moreover, as discussed above, the lower ignition temperature and early reaction onset for the Mg/B<sub>2</sub>O<sub>3</sub> mixture than Mg/CuO and B/CuO thermites suggests that Mg initiates the reaction with the oxide layer of B much earlier than its ignition and combustion with CuO. In the case of aluminum particles, similar pre-ignition reactions with its oxide shell (Al<sub>2</sub>O<sub>3</sub>) with reactive gases (e.g., HF and F<sub>2</sub>) have been shown to significantly affect their combustion.<sup>23,29</sup> Therefore, the low-temperature, pre-ignition Mg/B<sub>2</sub>O<sub>3</sub> surface reactions are expected to play a significant role in surface disruption and

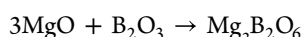
reactivity enhancement of boron, as discussed later in section 3.3.

To further characterize the reaction between Mg and B<sub>2</sub>O<sub>3</sub>, we performed TGA/DSC and XRD analyses on the Mg/B<sub>2</sub>O<sub>3</sub> mixtures. Figure 4a shows the TGA/DSC curves for the Mg/B<sub>2</sub>O<sub>3</sub> sample at a heating rate of 10 °C/min. The TGA curve shows ~22% mass loss at ~100–200 °C with two endothermic peaks appearing in the DSC signal. The mass loss and endotherms is attributed to the multi-step dehydration and decomposition of H<sub>3</sub>BO<sub>3</sub> present in the B<sub>2</sub>O<sub>3</sub> particles.<sup>30</sup> More importantly, we observe two distinct exotherms occurring at ~500–650 °C, indicating an exothermic redox reaction between Mg and B<sub>2</sub>O<sub>3</sub>. To understand the reaction mechanism, we heated the reaction mixture at different temperatures and analyzed the products by XRD characterization. As shown in Figure 4b, the unheated mixture shows characteristic peaks for both Mg and B<sub>2</sub>O<sub>3</sub>. The peaks remain unchanged up to a temperature of ~500 °C. However, when the samples are heated to a temperature of ~500 °C, the peaks for MgO begin to appear, while the B<sub>2</sub>O<sub>3</sub> and Mg peaks are highly diminished. At a higher temperature of ~650 °C, no B<sub>2</sub>O<sub>3</sub> and Mg peaks are observed, while MgO peaks are the most prominent (reaction approaching completion). At much higher temperatures (~1000 °C), peaks from ternary oxide, Mg<sub>3</sub>B<sub>2</sub>O<sub>6</sub>, appear, which likely forms because of an exothermic reaction between MgO and unreacted B<sub>2</sub>O<sub>3</sub> (Table 1). These results suggest that the Mg/B<sub>2</sub>O<sub>3</sub> reaction follows a two-step pathway: a magnesiothermic reduction of B<sub>2</sub>O<sub>3</sub> particles to boron (~500–600 °C), followed by the reaction of MgO and unreacted B<sub>2</sub>O<sub>3</sub> (>650 °C), as shown by the following reactions:

step I



step II



The Mg/B<sub>2</sub>O<sub>3</sub> redox reaction is further corroborated by the absence of BO<sub>x</sub> (BO<sub>3</sub>/BO<sub>4</sub>), O–H, and B–O–B peaks in the FTIR spectra of the Mg/B<sub>2</sub>O<sub>3</sub> mixtures heated at 650 °C, as shown in Figure 5. These results are also consistent with the DSC data shown in Figure 4a, where exothermic peaks were observed between ~500 and 650 °C. Moreover, the ignition temperature of the Mg/B<sub>2</sub>O<sub>3</sub> mixture in argon also occurs around similar temperatures (600 °C), as shown in Figure 3b. These observations confirm that the Mg/B<sub>2</sub>O<sub>3</sub> exothermic redox reaction occurs at relatively low temperatures of ~500–650 °C. Because these temperatures are higher than the melting point of B<sub>2</sub>O<sub>3</sub> (~450 °C), we postulate that Mg likely reacts with B<sub>2</sub>O<sub>3</sub> in a molten form, as discussed in the following sections.

**3.3. Mg/B<sub>2</sub>O<sub>3</sub> Reaction Mechanism: T-Jump/TOFMS and Implications on Oxide Shell Disruption of B NPs.** To further probe the interaction between Mg and B<sub>2</sub>O<sub>3</sub>, we analyzed the species evolved from the thermally activated Mg/B<sub>2</sub>O<sub>3</sub> reaction at a high heating rate (10<sup>5</sup> K/s) using T-jump/TOFMS, as described in section 2.4. Figure 6a shows the various species released from the Mg/B<sub>2</sub>O<sub>3</sub> samples. The most prominent gas-phase species evolved from the sample are H<sub>2</sub>O (*m/z* 18), Mg (*m/z* 24), and HOB<sub>2</sub>O species (*m/z* 45 and 62), as indicated in Figure 6a. A temporal profile of these species, shown in Figure 6b, reveals the mechanism of the Mg/B<sub>2</sub>O<sub>3</sub>

reaction. At low temperatures (~100–200 °C), desorption of adsorbed water and H<sub>3</sub>BO<sub>3</sub> decomposition results in the release of H<sub>2</sub>O and HOB<sub>2</sub>O fragments (H<sub>3</sub>BO<sub>2</sub> and H<sub>3</sub>BO<sub>3</sub>). At higher temperatures (~650 °C), we observe the release of gas-phase Mg species, as shown in Figure 6b. This result is consistent from a previous study of our group, where rapid Mg vaporization and release of gas-phase Mg species were observed.<sup>20</sup> Interestingly, the ignition of the Mg/B<sub>2</sub>O<sub>3</sub> samples (Figure 3b) occurs following B<sub>2</sub>O<sub>3</sub> melting and close to the release of vapor-phase Mg species, as demarcated in Figure 6b. These results suggest that the exothermic reaction between Mg/B<sub>2</sub>O<sub>3</sub> observed earlier (Figures 3–5) occurs by a heterogeneous reaction between vapor-phase Mg and molten B<sub>2</sub>O<sub>3</sub>, as illustrated later in Figure 8a. The Mg vapor-initiated heterogeneous reaction with the oxidizer surface (B<sub>2</sub>O<sub>3</sub>) is consistent with the reaction mechanism of Mg with the Bi<sub>2</sub>O<sub>3</sub> oxidizer observed in our previous study.<sup>20</sup> In this case, the redox reaction and ignition were similarly controlled by the release of Mg vapor, which reacted with the Bi<sub>2</sub>O<sub>3</sub> oxidizer surface and initiated ignition at the Mg vapor/oxidizer interface.

To investigate the effect of Mg directly on the B<sub>2</sub>O<sub>3</sub> oxide layer of boron NPs, a mixture of Mg and B NPs (~10 mol % Mg relative to the total mixture) was prepared without any oxidizer and DSC characterization was performed on the sample in ultrahigh-purity argon. Figure 7 shows the DSC curves of the Mg/B mixtures in argon compared to Mg/B<sub>2</sub>O<sub>3</sub> (Mg–boron oxide shell simulant mixture). Interestingly, we observe two Mg/B reaction exotherms around ~550–650 °C, the range observed earlier for the reaction between B<sub>2</sub>O<sub>3</sub> and Mg. Additionally, this temperature is higher than the melting point of the oxide shell (B<sub>2</sub>O<sub>3</sub>, 450 °C) and close to the Mg vapor release temperature observed earlier (~650 °C). Therefore, we conclude that the exotherms shown in the Mg/B DSC curve are likely a result of the heterogeneous reaction of Mg vapor with the molten oxide shell of boron NPs, as shown in Figure 8b. Note that, in addition to the reaction with the B<sub>2</sub>O<sub>3</sub> shell, excess Mg may undergo further reaction with boron to form borides in the absence of an oxidizer.

On the basis of the observations and the discussion above, we can extrapolate the reaction mechanisms of the Mg/B<sub>2</sub>O<sub>3</sub> system to Mg/B NP-based composites, whereby Mg vapor reacts with the molten B<sub>2</sub>O<sub>3</sub> shell, as illustrated in Figure 8. The Mg/B<sub>2</sub>O<sub>3</sub> reactions discussed in section 3.2 have several physical implications on the structure of the oxide surface of boron. First, the Mg vapor-induced reduction of B<sub>2</sub>O<sub>3</sub> to B possibly creates a pristine and accessible fuel surface for the reaction with the oxidizer. Second, further reaction of MgO with B<sub>2</sub>O<sub>3</sub> to nucleate ternary oxides, as seen in the XRD (Mg<sub>3</sub>B<sub>2</sub>O<sub>6</sub>; Figure 4b), in the B<sub>2</sub>O<sub>3</sub> liquid matrix may result in oxide shell thinning as a result of the wetting effects from the liquid around the solid oxide particles. Similar particle wetting effects have been observed in B/Bi<sub>2</sub>O<sub>3</sub> thermites and have been proposed to result in facilitated ignition.<sup>31</sup> These effects are expected to enhance the combustion of boron by increasing the accessible reactive fuel surface to the oxidizer. These effects are supported by the overlapping Mg, B, and O domains observed in the SEM–energy-dispersive X-ray spectroscopy (EDS) images of the combustion products of B/Mg/CuO composites (Figures S6 and S7 of the Supporting Information). Lastly, the exothermic reactions discussed in section 3.2 may also increase the local temperature of the unreacted B<sub>2</sub>O<sub>3</sub>

shell and assist in its physical vaporization and removal, thereby contributing to the reaction rate enhancement of boron particle oxidation. Prior studies have observed that reactive gas-phase species that can react with the  $B_2O_3$  shell can assist in its removal and lead to enhanced boron combustion.<sup>11,12,26</sup> With the assumption of a 50% reaction between Mg and the  $B_2O_3$  shell and further assumption that the exothermicity of the reaction is localized on the oxide shell (neglecting all heat losses), a simple energy balance yields an extremely high local surface temperature ( $T \sim 3200$  °C > boiling point of  $B_2O_3 \sim 1860$  °C), as described in section S8 of the Supporting Information. Of course, the actual temperature of the shell is expected to be considerably lower than this value as a result of the heat losses involved. Nevertheless, the estimates and the observations above suggest that the Mg/ $B_2O_3$  (oxide shell) reaction system possesses sufficient energy required for the vaporization of the molten  $B_2O_3$  layer. These results indicate that additional surface reactions related to the interaction of Mg with the oxide shell of boron particles contribute significantly to their reactivity enhancement and need to be taken into consideration for Mg/B-based energetic systems.

#### 4. CONCLUSION

In this work, we explored the effect of Mg particles as an additive secondary fuel on the reactivity of B-based composites. Specifically, we investigated the exothermic reaction mechanism between Mg and  $B_2O_3$  and its consequences on the reaction rate of B/CuO composites. We demonstrate that incorporating nanoscale Mg as an additive fuel in B/CuO composites leads to a ~6-fold increase in reactivity (pressurization rates), while the burn time of the composites is shortened by ~60%. We further studied the reaction mechanism of Mg/ $B_2O_3$  particles as a simulant system for the interaction of Mg with the  $B_2O_3$  shell of boron. Thermal and reaction product analysis, along with T-jump/TOFMS and ignition characterization, suggests that Mg vapor undergoes several heterogeneous reactions with the molten  $B_2O_3$  shell of boron at relatively low temperatures. These surface reactions occur prior to the ignition of B with CuO and likely cause surface disruptions in the oxide shell, contributing to the observed enhanced reactivity of B composites.

#### ■ ASSOCIATED CONTENT

##### SI Supporting Information

The Supporting Information is available free of charge at <https://pubs.acs.org/doi/10.1021/acs.energyfuels.2c02347>.

Particle sizes of as-received boron NPs and synthesized Mg NPs (section S1), TGA and active content of boron and Mg fuels (section S2), ball milling of  $B_2O_3$  particles and particle size obtained (section S3), compositional details of the fabricated mixtures (section S4), pressurization and optical traces of thermite composites (section S5), ignition snapshots of B/Mg/CuO thermites in argon (section S6), combustion product characterization (section S7), and estimation of the temperature rise after reaction of Mg vapor with the  $B_2O_3$  shell of B NPs (section S8) (PDF)

#### ■ AUTHOR INFORMATION

##### Corresponding Authors

Michael R. Zachariah – University of California, Riverside, Riverside, California 92507, United States; [orcid.org/0000-0002-4115-3324](https://orcid.org/0000-0002-4115-3324); Email: [mrz@engr.ucr.edu](mailto:mrz@engr.ucr.edu)

Reza Abbaschian – University of California, Riverside, Riverside, California 92507, United States; Email: [rabba@engr.ucr.edu](mailto:rabba@engr.ucr.edu)

##### Authors

Pankaj Ghildiyal – University of California, Riverside, Riverside, California 92507, United States; University of Maryland, College Park, Maryland 20742, United States; [orcid.org/0000-0002-4422-3068](https://orcid.org/0000-0002-4422-3068)

Feiyu Xu – University of California, Riverside, Riverside, California 92507, United States; University of Maryland, College Park, Maryland 20742, United States

Alex Rojas – University of California, Riverside, Riverside, California 92507, United States

Yujie Wang – University of California, Riverside, Riverside, California 92507, United States

Mahbub Chowdhury – University of California, Riverside, Riverside, California 92507, United States

Prithwish Biswas – University of California, Riverside, Riverside, California 92507, United States; [orcid.org/0000-0002-9921-2905](https://orcid.org/0000-0002-9921-2905)

Steven Herrera – University of Maryland, College Park, Maryland 20742, United States

Complete contact information is available at: <https://pubs.acs.org/doi/10.1021/acs.energyfuels.2c02347>

##### Notes

The authors declare no competing financial interest.

#### ■ ACKNOWLEDGMENTS

This work is supported by the Defense Threat Reduction Agency (DTRA)–University Research Alliance (URA) on Materials under Extreme Conditions and the Office of Naval Research (ONR).

#### ■ REFERENCES

- Jiang, Y.; Deng, S.; Hong, S.; Zhao, J.; Huang, S.; Wu, C.-C. L.; Gottfried, J.; Nomura, K.; Li, Y.; Tiwari, S.; et al. Energetic Performance of Optically Activated Aluminum/Graphene Oxide Composites. *ACS Nano* **2018**, *12* (11), 11366–11375.
- Dreizin, E. L. Metal-Based Reactive Nanomaterials. *Prog. Energy Combust. Sci.* **2009**, *35*, 141–167.
- Rehboldt, M. C.; Yang, Y.; Wang, H.; Holdren, S.; Zachariah, M. R. Ignition of Nanoscale Titanium/Potassium Perchlorate Pyrotechnic Powder: Reaction Mechanism Study. *J. Phys. Chem. C* **2018**, *122* (20), 10792–10800.
- Wang, J.; Zhang, L.; Shen, J.; Li, Z. Highly Reactive PTFE/Mg Nanolaminates and Its Combustion Performances. *Adv. Mater. Interfaces* **2019**, *6* (14), 1900113.
- Valluri, S. K.; Schoenitz, M.; Dreizin, E. Bismuth Fluoride-Coated Boron Powders as Enhanced Fuels. *Combust. Flame* **2020**, *221*, 1–10.
- Chintersingh, K. L.; Sun, Y.; Schoenitz, M.; Dreizin, E. L. Heterogeneous Reaction Kinetics for Oxidation and Combustion of Boron. *Thermochim. Acta* **2019**, *682*, 178415.
- Yeh, C. L.; Kuo, K. K. Ignition and Combustion of Boron Particles. *Prog. Energy Combust. Sci.* **1996**, *22* (6), 511–541.

- (8) Mursalat, M.; Schoenitz, M.; Dreizin, E. L. Effect of Particle Morphology on Reactivity, Ignition and Combustion of Boron Powders. *Fuel* **2022**, *324*, 124538.
- (9) Jain, A.; Joseph, K.; Anthonyamy, S.; Gupta, G. S. Kinetics of Oxidation of Boron Powder. *Thermochim. Acta* **2011**, *514* (1–2), 67–73.
- (10) Chintersingh, K. L.; Schoenitz, M.; Dreizin, E. L. Oxidation Kinetics and Combustion of Boron Particles with Modified Surface. *Combust. Flame* **2016**, *173*, 288–295.
- (11) Baek, J.; Jiang, Y.; Demko, A. R.; Jimenez-Thomas, A. R.; Vallez, L.; Ka, D.; Xia, Y.; Zheng, X. Effect of Fluoroalkylsilane Surface Functionalization on Boron Combustion. *ACS Appl. Mater. Interfaces* **2022**, *14* (17), 20190–20196.
- (12) Wang, J.; Mao, Y.; Chen, J.; Li, Z. J.; Wang, J.; Nie, F. Surface Engineering Boron/Graphite Fluoride Composite with Enhanced Ignition and Combustion Performances. *Fuel* **2022**, *323*, 124374.
- (13) Valluri, S. K.; Schoenitz, M.; Dreizin, E. Boron-Metal Fluoride Reactive Composites: Preparation and Reactions Leading to Their Ignition. *J. Propuls. Power* **2019**, *35* (4), 802–810.
- (14) Abraham, A.; Obamedo, J.; Schoenitz, M.; Dreizin, E. L. Effect of Composition on Properties of Reactive Al-B-I<sub>2</sub> Powders Prepared by Mechanical Milling. *J. Phys. Chem. Solids* **2015**, *83*, 1–7.
- (15) Zhang, B.; Huang, C.; Yan, S.; Li, Y.; Cheng, Y. Enhanced Reactivity of Boron, through Adding Nano-Aluminum and Wet Ball Milling. *Appl. Surf. Sci.* **2013**, *286*, 91–98.
- (16) Liu, J. Z.; Xi, J. F.; Yang, W. J.; Hu, Y. R.; Zhang, Y. W.; Wang, Y.; Zhou, J. H. Effect of Magnesium on the Burning Characteristics of Boron Particles. *Acta Astronaut.* **2014**, *96* (1), 89–96.
- (17) Hashim, S. A.; Karmakar, S.; Roy, A. Effects of Ti and Mg Particles on Combustion Characteristics of Boron-HTPB-Based Solid Fuels for Hybrid Gas Generator in Ducted Rocket Applications. *Acta Astronaut.* **2019**, *160*, 125–137.
- (18) Xu, F.; Biswas, P.; Nava, G.; Schwan, J.; Kline, D. J.; Rehwoldt, M. C.; Mangolini, L.; Zachariah, M. R. Tuning the Reactivity and Energy Release Rate of I<sub>2</sub>O<sub>5</sub> Based Ternary Thermite Systems. *Combust. Flame* **2021**, *228*, 210–217.
- (19) Zhao, W.; Wang, X.; Wang, H.; Wu, T.; Kline, D. J.; Rehwoldt, M.; Ren, H.; Zachariah, M. R. Titanium Enhanced Ignition and Combustion of Al/I<sub>2</sub>O<sub>5</sub> Mesoparticle Composites. *Combust. Flame* **2020**, *212*, 245–251.
- (20) Ghildiyal, P.; Biswas, P.; Herrera, S.; Xu, F.; Alibay, Z.; Wang, Y.; Wang, H.; Abbaschian, R.; Zachariah, M. R. Vaporization-Controlled Energy Release Mechanisms Underlying the Exceptional Reactivity of Magnesium Nanoparticles. *ACS Appl. Mater. Interfaces* **2022**, *14* (15), 17164–17174.
- (21) Liu, X.; Chintersingh, K. L.; Schoenitz, M.; Dreizin, E. L. Reactive Composite Boron-Magnesium Powders Prepared by Mechanical Milling. *J. Propuls. Power* **2018**, *34* (3), 787–794.
- (22) Ghildiyal, P.; Ke, X.; Biswas, P.; Nava, G.; Schwan, J.; Xu, F.; Kline, D. J.; Wang, H.; Mangolini, L.; Zachariah, M. R. Silicon Nanoparticles for the Reactivity and Energetic Density Enhancement of Energetic-Biocidal Mesoparticle Composites. *ACS Appl. Mater. Interfaces* **2021**, *13* (1), 458–467.
- (23) Delisio, J. B.; Hu, X.; Wu, T.; Egan, G. C.; Young, G.; Zachariah, M. R. Probing the Reaction Mechanism of Aluminum/Poly(Vinylidene Fluoride) Composites. *J. Phys. Chem. B* **2016**, *120* (24), 5534–5542.
- (24) Keerthi, V.; Nie, H.; Pisharath, S.; Hng, H. H. Combustion Characteristics of Fluoropolymer Coated Boron Powders. *Combust. Sci. Technol.* **2022**, *194* (6), 1183–1198.
- (25) Wang, S.; Liu, X.; Schoenitz, M.; Dreizin, E. L. Nanocomposite Thermite with Calcium Iodate Oxidizer. *Propellants, Explos. Pyrotech.* **2017**, *42* (3), 284–292.
- (26) Xi, J.; Liu, J.; Wang, Y.; Liang, D.; Li, H.; Zhou, J. Role of Oxalic Acid in Promoting Ignition and Combustion of Boron: An Experimental and Theoretical Study. *Propellants, Explos. Pyrotech.* **2014**, *39* (6), 844–851.
- (27) National Institute of Standards and Technology (NIST). *NIST Chemistry WebBook*, SRD 69; NIST: Gaithersburg, MD, 2022; <https://webbook.nist.gov>.
- (28) The Materials Project. <https://materialsproject.org> (accessed Oct 3, 2022).
- (29) Li, Y.; Li, J.; Wang, B.; Ma, H.; Han, Z. An Approach to the Induced Reaction Mechanism of the Combustion of the Nano-Al/PVDF Composite Particles. *Surf. Coat. Technol.* **2022**, *429*, 127912.
- (30) Huber, C.; Jahromy, S. S.; Birkelbach, F.; Weber, J.; Jordan, C.; Schreiner, M.; Harasek, M.; Winter, F. The Multistep Decomposition of Boric Acid. *Energy Sci. Eng.* **2020**, *8* (5), 1650–1666.
- (31) Wang, X.; Wu, T.; Wang, H.; DeLisio, J. B.; Yang, Y.; Zachariah, M. R. Boron Ignition and Combustion with Doped  $\delta$ -Bi<sub>2</sub>O<sub>3</sub>: Bond Energy/Oxygen Vacancy Relationships. *Combust. Flame* **2018**, *197*, 127–133.

## Recommended by ACS

### Breaking of Water-in-Crude Oil Emulsions. 10. Experimental Evidence from a Quartz Crystal Resonator Sensor and an Oscillating Spinning Drop Interfacial Rhe...

Ronald Marquez, Jean-Louis Salager, *et al.*

JANUARY 27, 2023  
ENERGY & FUELS

READ 

### Intelligent Method to Optimize the Frequency Modulation for Beam Pumping System Based on Deep Reinforcement Learning

Ruichao Zhang, Liangfei Xiao, *et al.*

MARCH 02, 2023  
ACS OMEGA

READ 

### Investigation of Foam Flooding Assisted by Non-Newtonian and Novel Newtonian Viscosifying Agents for Enhanced Oil Recovery

Seyed Mojtaba Hosseini-Nasab, Pacelli L. J. Zitha, *et al.*

DECEMBER 23, 2022  
ACS OMEGA

READ 

### Nitrogen-Doping-Induced High-Performance Carbon Nanofiber Anodes for Potassium-Ion Storage

Yu-Lin Bai, Kai-Xue Wang, *et al.*

FEBRUARY 09, 2023  
ACS APPLIED NANO MATERIALS

READ 

Get More Suggestions >